



Construction of CdS/CoO_x core-shell nanorods for efficient photocatalytic H₂ evolution



Ye Liu^a, Shuoping Ding^a, Yiqiu Shi^a, Xiufan Liu^a, Zuozuo Wu^a, Qingqing Jiang^a, Tengfei Zhou^{a,b}, Nikang Liu^a, Juncheng Hu^{a,*}

^a Key Laboratory of Catalysis and Materials Science of the State Ethnic Affairs Commission & Ministry of Education, South-Central University for Nationalities, Wuhan, 430074, China

^b Key Laboratory of Advanced Energy Materials Chemistry (Ministry of Education), Nankai University, Tianjin 300071, China

ARTICLE INFO

Keywords:
CdS/CoO_x
Core-shell
Photocatalysis
H₂ evolution

ABSTRACT

Efficient separation of electrons and holes, associated with the reduction or oxidation reactions, is of great significance in a photocatalytic system. In this study, we demonstrate the novel CdS/cobalt oxide core-shell nanorods (CdS/CoO_x core-shell NRs) prepared by a facile impregnation-calcination method. The negatively charged surface of CdS induces the in situ growth of CoO and Co₃O₄ (abbreviated as CoO_x here) as the outer shell, which efficiently captures the photogenerated holes and renders drastically improved charge separation efficiency to CdS/CoO_x core-shell NRs. Moreover, the intimate interfacial contact between the CdS core and CoO_x shell offers rectified charge transfer directions, which further boosts the charge separation. In consequence, the severe photocorrosion is effectively alleviated, and nearly ca. 43-folds higher of H₂ production rate is achieved on CdS/CoO_x core-shell NRs compared to the pristine CdS NRs. We believe that this work not only provides new approaches toward photocatalysts with steerable charge flows and enhanced photostability, but also contributes to design other efficient photocatalytic systems.

1. Introduction

Driven by the promise of developing an ideal vector of sustainable energy, semiconductor based photocatalytic water splitting is drawing enormous attention among researchers [1–4]. The production of H₂ from water using sunlight-activated semiconductors forms a fundamental concept for clean and renewable alternatives, in which sunlight is almost inexhaustible and the combustion product only contains water [5–7]. In semiconductor nanocrystals, electron-hole pairs generate on the absorption of photons with energy higher than the band gap, followed by subsequent charge separation and migration to the surface of photocatalysts for oxidation or reduction reactions [8,9]. CdS, as a typical visible-light driven photocatalyst, was considered as one of the most promising candidates for water splitting owing to its suitable band gap potentials [10]. However, the photocatalytic activities of CdS are far more exciting due to the severe photocorrosion and rapid recombination of photogenerated electron-hole pairs [11,12]. In view of this, strategies have been implemented to promote the photocatalytic activities of CdS. For example, Luo et al. reported that CdS nanospheres with a hollow interior could dramatically improve the photocatalytic activities toward contaminants degradation [13]. Yang and his co-

workers found that Zn doped CdS architectures exhibit much higher photoactivities and stability under visible light [14]. Recently, researchers discovered that the photocatalytic activities of CdS were greatly enhanced through depositing co-catalysts on CdS, typically, Simon and his co-workers developed Ni-decorated CdS nanorods with much higher photoactivities than that of pristine CdS nanorods [11], this tends to be more effective than the previously reported two strategies, indicating that co-catalysts deposition could be one of the most prominent methods toward improving the activity and stability of CdS.

Proper selection of co-catalysts is significant in creating an efficient photocatalytic system as mentioned above. A promising co-catalyst should possess large work function for electron sinks, or lowering the over potential for hole transportation [15,16]. Yamakata et al. and Li et al. discovered that CoO_x co-catalyst could effectively capture holes in a few picoseconds, therefore the life time of both electrons and holes were prolonged dramatically [17,18]. Later literatures reported that CoO_x loaded photocatalysts showed relatively much higher water oxidation activity than their individual analogues, in which CoO_x played significant roles of hole capturing and hindering the recombination of electrons and holes [19,20]. Therefore, CoO_x could be a promising candidate co-catalyst for water splitting. Despite the tremendous efforts

* Corresponding author.

E-mail address: jchu@mail.scuec.edu.cn (J. Hu).

devoted to the effect of CoO_x on water oxidation reactions, the corresponding strategies focused on improving the photocatalytic hydrogen evolution activities, yet have been barely reported.

Nevertheless, choosing a suitable strategy to load co-catalysts on semiconductors is also important in improving the overall efficiency of a photocatalytic system. For example, spatially loaded co-catalysts or rationally designed junctions were more favorable for charge separation owing to the accumulated active sites and rectified charge transportation pathways, while randomly deposited co-catalysts result in a random flow of charges and a corresponding high recombination rate of electron-hole pairs [21,22,23]. In consequence, it is indispensable to design suitable strategies for the deposition of co-catalysts, among which the construction of core/shell nanostructures could be taken as a proof-of-concept according to the previously reported literatures [21,22,24,25].

Herein, we establish an efficient photocatalytic system by crafting hole capturing CoO_x layer onto semiconducting CdS NRs, which results in a novel core-shell structure with intimately contacted interfaces. Specifically, the negatively charged surface of CdS NRs acts as a matrix for adsorbing Co^{2+} ions through electrostatic interaction, leading to the in situ growth of CoO and Co_3O_4 in the outer shell. Due to the hole capture effect of CoO_x and the intimately contacted CoO_x shell, photogenerated electrons and holes are directionally transported to CdS NRs and the CoO_x layer, respectively, thereby the charge separation efficiency is greatly improved. As a consequence, the illustrational CdS/CoO_x core-shell NRs possess more superior photostability under visible light illumination ($\lambda > 420$ nm), and correspondingly exhibits *ca.* 43-folds faster of H_2 evolution rate than the pristine CdS NRs. The feasibility and reproducibility of this strategy offers a new way of designing photocatalysts with optimized charge separation and enhanced stability, and is expected to design other solar energy conversion systems.

2. Experimental

2.1. Reagents

All the chemicals, including ethylenediamine ($\text{C}_2\text{H}_4(\text{NH}_2)_2$), cadmium chloride hemipentahydrate ($\text{CdCl}_2 \cdot 2.5\text{H}_2\text{O}$), cobalt nitrate hexahydrate ($\text{Co}(\text{NO}_3)_2 \cdot 6\text{H}_2\text{O}$), thiourea (NH_2CSNH_2), and ethanol were purchased from Sinopharm Chemical Reagent Co., Ltd. (Shanghai, China). All of the reagents were analytical grade and used as received without any further purification.

2.2. Synthesis of CdS nanorods (CdS NRs)

In a typical synthesis, 2.313 g of cadmium chloride hemipentahydrate and 2.31 g of thiourea were dispersed in 30 ml ethylenediamine, followed by 40 min of ultrasonic stirring, then the mixture was transferred to a Teflon-lined stainless steel autoclave with a capacity of 100 ml and maintained at 160 °C for 48 h. After the solvothermal process, the obtained product was collected by filtration and washed with de-ionized water and absolute ethanol to remove the residual ions. The resultant yellow-colored powders were collected and dried at 60 °C overnight.

2.3. Synthesis of CdS/CoO_x core-shell NRs

Detailedly, 0.1 g of CdS NRs were dispersed in 60 ml of ethanol containing a designed amount of $\text{Co}(\text{NO}_3)_2 \cdot 6\text{H}_2\text{O}$ (5 mg, 10 mg, 20 mg and 40 mg for sample CC-5, CC-10, CC-20 and CC-40, respectively). After 10 min of sonication, the mixture was magnetic stirred until ethanol had been thoroughly volatilized. Finally, the CdS NRs impregnated with Co^{2+} were placed in an aluminum crucible with a cover, and calcinated under 400 °C for 2 h in ambient conditions with a ramping rate of 2 °C per minute. The resultant products were collected for further characterization.

2.4. Synthesis of CdS NRs with randomly deposited CoO_x

Randomly distributed CoO_x (CCM) was prepared by simply remix the decomposition product of $\text{Co}(\text{NO}_3)_2 \cdot 6\text{H}_2\text{O}$ and CdS NRs. Briefly, a mixture of 0.1 g CdS NRs and stoichiometric amount of $\text{Co}(\text{NO}_3)_2 \cdot 6\text{H}_2\text{O}$ (calculated on the basis of the molar ratio of cobalt in sample CC-20) was placed in a aluminum crucible and calcinated under the same conditions as that in the synthesis of CdS/CoO_x core-shell NRs. Accordingly, the bulk CoO_x sample was synthesized by direct thermal annealing cobalt nitrate hexahydrate. Then the resultant products was collected and milled into powder in a mortal.

3. Characterization

The powder X-ray diffraction (XRD) (Bruker D8 Advance; $\text{Cu K}\alpha = 1.5404$ Å) was utilized to analyze the crystalline structure of the as-prepared samples. The 2θ range was from 10° to 80° with a scanning rate of 0.05°/s. The microstructure and size of the samples were investigated by SU8010 field-emission scanning electron microscope (FESEM, Hitachi, Japan) at a decelerating voltage 2 kV. Energy dispersive spectrum (EDS) was connected to FESEM. Transmission electron microscope (TEM) and high resolution trans-mission electron microscopy(HRTEM) were obtained on a JEOL 2100-F (JEOL, Japan) microscope operated at an accelerating voltage of 200 kV, the sample powder was evenly dispersed into ethanol by ultrasonic treatment and dropped a very dilute suspension onto a copper grid. HAADF-STEM and the corresponding EDX data was conducted on FEI Titan Themis 200 equipped with Bruker Super-X. Zeta potentials of the pristine CdS NRs was recorded on a Zeta sizer Nano S90 (Malvern, England) device. X-ray photoelectron spectroscopy(XPS) was recorded on a VG Multi lab 2000 (VG Inc.) photoelectron spectrometer using monochromatic Al $\text{K}\alpha$ radiation as the excitation source under vacuum at 2×10^{-6} Pa. All the binding energies were referenced to the C 1s peak at 284.8 eV of the surface adventitious carbon. The UV-vis diffused reflectance spectra (DRS) were tested with a Cary Series UV-vis–NIR Spectrophotometer (Agilent Technologies) from 200 to 2000 nm by a diffuse reflectance method using polytetrafluoroethylene as a reference materials. Photoluminescence (PL) measurements were carried out at room temperature in a Hitachi F-7000 with a 150 W Xe lamp. The samples were excited at 332 nm, and the emission filter (300–800 nm) was used to minimize the background single at the excitation wavelength. Photocurrent measurements were taken on a Ivium workstation (Ivium Stat.h, Ivium Holland, Inc.) without bias in 0.5 M aqueous Na_2SO_4 solution electrolyte without any additive. The visible light source (460 nm) was provided by a LED light (Ivium IM5115) as an accessory of the Ivium workstation. Electrochemical impedance spectra (EIS) was performed by an electrochemical system (CHI-660e, CHI Shanghai, Inc.) in three-electrode quartz cells with 5.0 mM $\text{K}_3[\text{Fe}(\text{CN})_6]/\text{K}_4[\text{Fe}(\text{CN})_6]$ electrolyte solution, and platinum wire was used as the counter electrode, saturated calomel electrodes (SCE) were used as the reference electrodes by applying an ac voltage with 1.6 mV amplitude in a frequency range from 1 Hz to 85 kHz under open circuit potential conditions. The tests were performed at a 1.6 mV of alternating current signal in the frequency range of 1–105 Hz and the data obtained were fitted using ZSimpWin software.

3.1. Photocatalytic activity test

All the photocatalytic tests were carried out under N_2 atmosphere with a 350 W xenon lamp equipped with a 420 nm cutoff filter to simulate visible light. For the evolution of hydrogen, 0.04 g of the photocatalyst and 100 ml of aqueous solution containing 0.35 M Na_2S and 0.25 M Na_2SO_3 as sacrificial agents were placed in a quartz reactor, then the mixture was stirred and purged with nitrogen for 30 min to remove the air before light irradiation. The reactor was equipped with water circulation in the outer interlayer to alleviate the influence

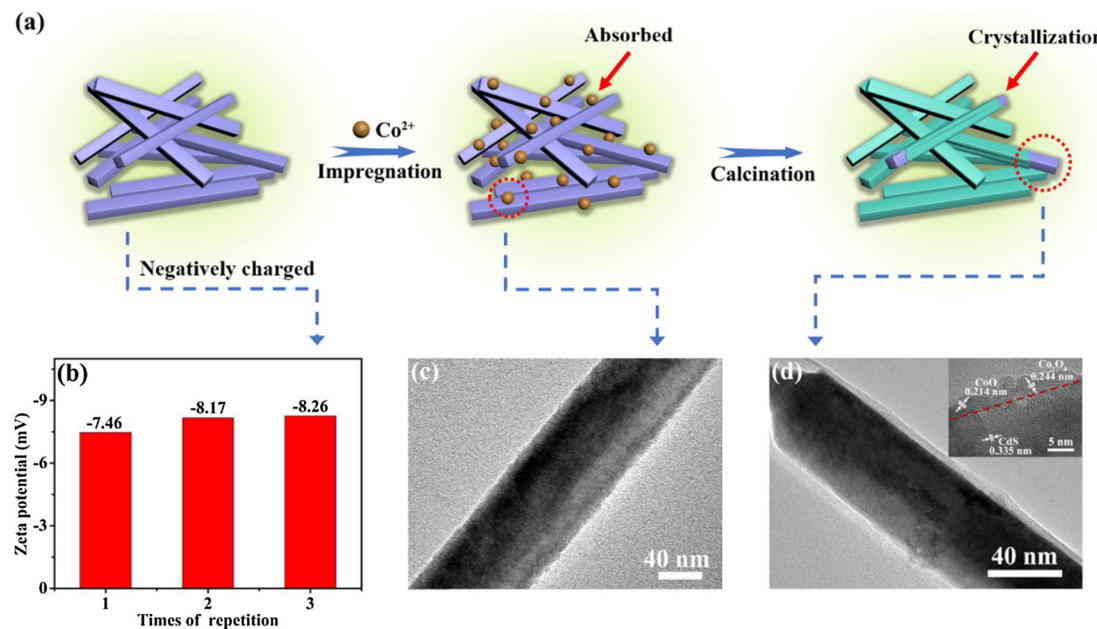


Fig. 1. a) Schematic illusion for the formation of the CdS/CoO_x core-shell NRs. b) Zeta potential of pristine CdS NRs. c) TEM image of CdS NRs after impregnation. d) TEM image of CC-20, the inset is the corresponding HRTEM image.

brought by the heat from light. During the photocatalytic tests, 0.4 ml of sample gas was taken out each 60 min by a gas injector, and the concentration of H₂ was monitored by a gas chromatography (FULI 9790).

The cycling experiments were performed as follows. In a typical run, the photocatalyst after 6 h of H₂ generation were centrifuged, rinsed and dried at 60 °C, the quartz reactor was degassed and placed with photocatalyst and sacrificial agents as the above photocatalytic H₂ evolution tests. Similarly, the following three runs were performed with the same procedures.

4. Results and discussion

The fabrication of CdS/CoO_x core-shell NRs is schematically illustrated in Fig. 1a. In the initial stage, the surface of the hydrothermally prepared CdS NRs is negatively charged with an average Zeta potential of -7.96 mV (Fig. 1b), which is favorable of absorbing positively charged Co²⁺ ions through electrostatic interaction via the subsequent impregnation process. FESEM images in Fig. S1a, b show typical 1D rod-like morphology of the pristine CdS NRs and CdS NRs after impregnation, respectively. Obviously, no extrinsic species are observed after impregnation, which can be further confirmed by the corresponding TEM image in Fig. 1c. Since the pristine CdS NRs pronounce negatively charged Zeta potentials, the positively charged Co²⁺ can be strongly immobilized onto the surface of CdS NRs. The subsequent calcination process in static air could result in the partial oxidation of Co²⁺ and confine the crystallized cobalt oxides onto the surface of CdS NRs, directing the epitaxial growth of cobalt oxides. Consequently, as the FESEM image shown in Fig. S1c, a relatively rougher surface is found on CC-20 comparing to the pristine CdS NRs, which provides the preliminary evidence of the CoO_x outer shell. TEM image of CC-20 in Fig. 1d shows more convincible evidence for it, as can be clearly seen that the 1D morphology is well preserved, while an obvious outer shell with distinct interface between the CdS core and CoO_x shell is observed, confirming the formation of the core-shell structure. Furthermore, high-resolution transmission electron microscope (HRTEM) image in the inset picture of Fig. 1d reveals the crystal structures of the samples, the fringes with lattice spacing of 0.335 nm matches well with the (002) plane of hexagonal CdS. And the lattice spacing of about 0.244 nm in the outer layer could be assigned as the (311) plane of cubic Co₃O₄, while a

friction of lattice spacing of 0.214 nm corresponds well with the (200) plane of cubic Co[26].

To investigate the elemental distribution on CC-20, the high-angle annular dark-field scanning TEM-energy dispersive spectroscopy (HAADF-STEM-EDX) was conducted. As is shown in Fig. 2b–e, the overall distribution of Co and O is observed, further demonstrating that the CoO_x outer shell has been successfully deposited on to the surface of CdS NRs.

The crystallographic nature of the samples are examined by powder X-ray diffraction (XRD). As is shown in Fig. 3a, the diffraction peaks of pristine CdS NRs can be readily assigned to the hexagonal crystallite CdS (JCPDS card No. 77-2306), indicating the high purity of the as-prepared CdS NRs. The XRD pattern of CdS NRs after calcination in Fig. S2 verifies the unchanged crystal phase after the calcination process. Interestingly, no obvious diffraction peaks of cobalt species are observed in any of the samples, and the baseline of the XRD patterns are broadened as the content of the impregnated Co²⁺ increases, which is possibly in consequence of the pure crystallinity and uniform distribution of CoO_x[27,28].

Further investigations from the standpoints of electron states and elemental compositions are carried out in order to better understand the interactions between CoO_x and CdS NRs, as depicted in the high-resolution X-ray photoelectron spectroscopy (XPS) spectra. It can be seen from the survey scan results of sample CC-20 in Fig. 3b that it mainly consists of two elements, namely Cd and S. Additionally, weak peaks of CoO_x are also detected due to the relatively low content. As is shown in Fig. 3c, the binding energies corresponding to Cd 3d_{3/2} and Cd 3d_{5/2} for divalent cadmium (Cd²⁺) appear at 411.4 eV and 404.7 for CdS, respectively[29,30]. And the binding energies located at 410.8 eV and 404.1 eV could be assigned as Cd 3d_{3/2} and Cd 3d_{5/2} in low valance state or interstitial Cd[31,32,33]. In the meanwhile the two deconvoluted peaks associated with S 2p 162.6 eV (S 2p_{1/2}) and 161.5 eV (S 2p_{3/2}) are certified as typical characteristic peaks of S²⁻ in CdS (Fig. 3d)[10,24]. It is worth noting that the peaks of both Cd 3d and S 2p shift toward higher binding energies for about 0.8 eV compared to the pristine CdS NRs, revealing the strong interaction formed between the interface of the two species[34,35]. Considerations must be taken to analyze the XPS results of cobalt 2p core levels because of the close binding energies of the cobalt oxidation states, multiplet splitting, and the presence of satellites. The surface chemical states of cobalt can be

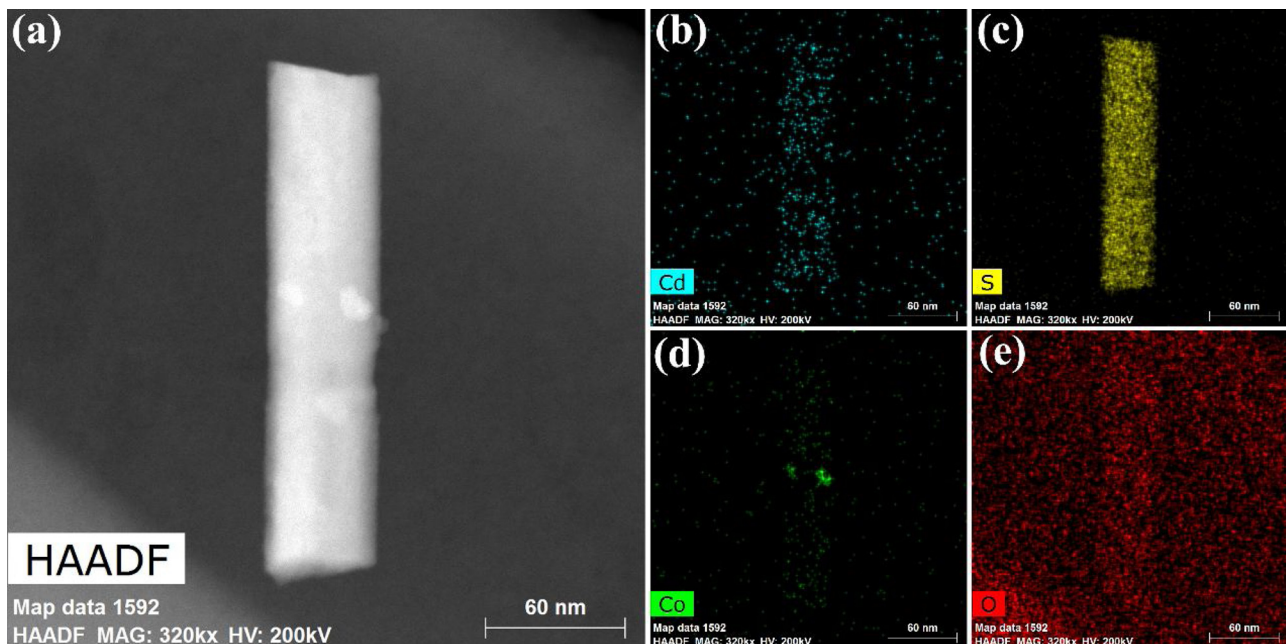


Fig. 2. a) HAADF-STEM image of sample CC-20. b-e) The corresponding EDX elemental mapping analysis.

easily justified by their satellite peaks rather than their main core levels [36]. Detailedly, the satellite peak near the $2p_{3/2}$ state for Co_3O_4 is higher than that of CoO , whereas the satellite peak of the $2p_{1/2}$ state for Co_3O_4 is slightly lower than that of CoO [19]. As shown in Fig. S3a, the binding energies at 780.3 eV and 795.3 eV of Co $2p_{3/2}$ and $2p_{1/2}$ differ from the single phase of CoO or Co_3O_4 , instead, the two main peaks can be assigned as Co_3O_4 [37], while the two satellite peaks can be readily regarded as the characteristics of CoO [38]. Moreover, the deconvoluted shoulder peaks of O 1s located at 532.5 eV, 531.6 eV and 530.8 eV

could be assigned as metal oxides and the surface absorbed O- or OH- (Fig. S3b) [39,40,41]. These results confirm that the cobalt oxides are identified to be the coexistence of nanocrystalline CoO and Co_3O_4 [26,42,43], which is in agreement with the TEM analysis.

As shown in Fig. 4a, UV-vis diffuse reflectance spectra (DRS) is conducted to investigate the optical properties of the samples, whereby the light absorption properties of a photocatalyst can be unambiguously examined. The absorption edge of pristine CdS lying at around 525 nm can be assigned to be the intrinsic band gap absorption of CdS

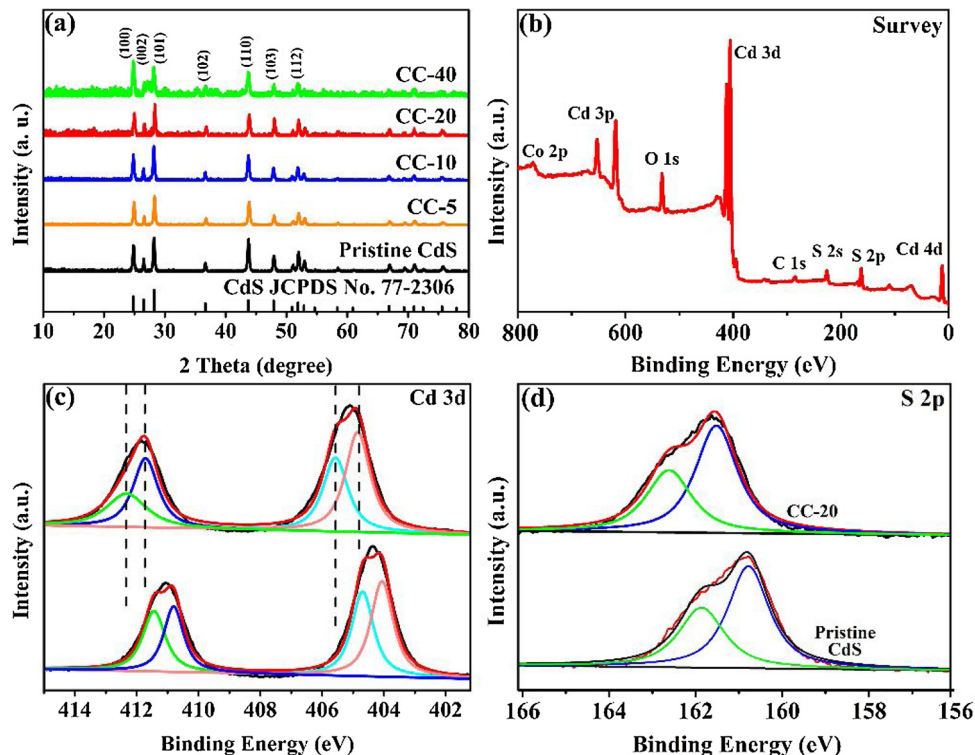


Fig. 3. Structural and compositional characterizations of the photocatalysts. a) XRD patterns. b) Survey of the XPS spectra of CC-20. c-d) The corresponding high-resolution XPS spectra of Cd 3d and S 2p.

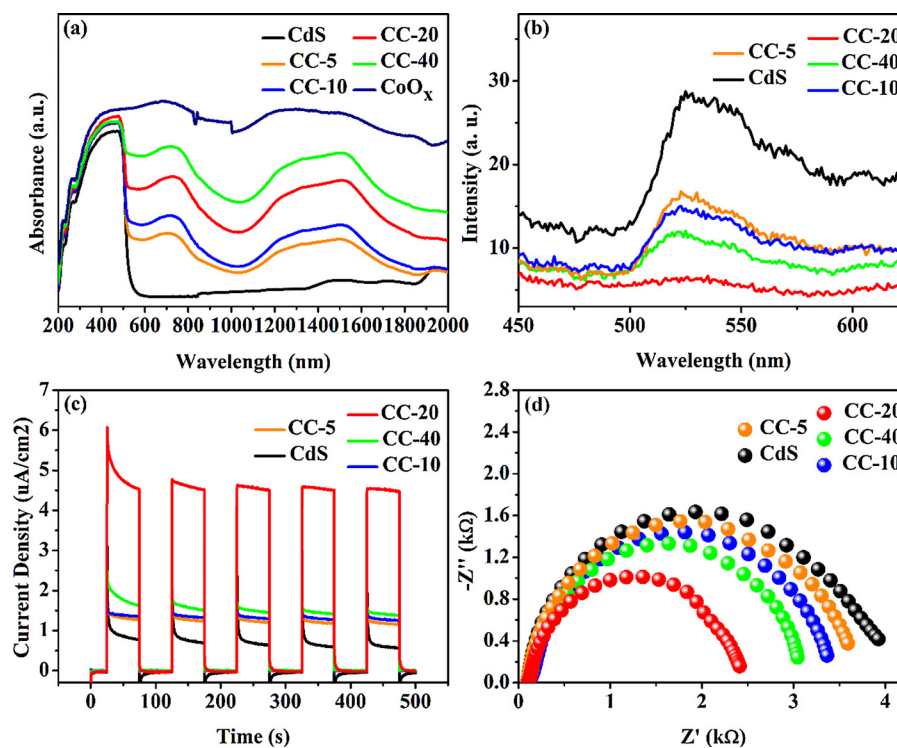


Fig. 4. a) UV-vis diffuse reflectance (DRS) spectra of the samples. b) Photoluminescence (PL) spectra of the samples. c) Transient photocurrent response under visible light irradiation and d) electrochemical impedance spectroscopy (EIS) of the samples.

according to the previously reported literature [44]. Besides, the peaks corresponding to typical Co_3O_4 transitions are also observed in each sample except pristine CdS NRs, they are: crystal field $^4\text{A}_2(\text{F}) \rightarrow ^4\text{T}_1(\text{F})$ transitions at 1460 nm, an “intervalence” charge-transfer $\text{Co}^{2+} \rightarrow \text{Co}^{3+}$ representing an internal oxidation-reduction process at 1220 nm, and ligand-metal charge transfer events $\text{O}^{2-} \rightarrow \text{Co}^{3+}$ at 657 nm [45,46]. Interestingly, reinforced optical absorption is observed in both visible-light region and even near infrared region for CdS/CoO_x core-shell NRs compared to pristine CdS NRs, which is in accordance with the color variations (from yellow to grey, Fig. S5) in sample CdS and CC5-CC40. Strengthened light-absorption in such wide spectrum impedes light reflection and harvests more incident photons into photocatalytic reaction process, which may result in an elevated photoactivity to some extent. As the magnified DRS spectra in Fig. S4a shows, the absorption edge in the visible light region (~ 520 nm) exhibits an apparent redshift as the amount of the deposited CoO_x increases. It may be due to the fact that the photogenerated holes are captured by CoO_x and electrons are left in CdS NRs [17,18,47], engendering an electron-rich state and reduces the electron transition energy in CdS/CoO_x photocatalyst [48].

It has been generally accepted that the optical absorption property of photocatalyst is closely correlated with its band gap. And band gap energies of the samples can be estimated by extrapolating the straight portion of plot to $\alpha = 0$ based on the formula: $a\hbar\nu = A(\hbar\nu - Eg)n/2$, where Eg , ν , h , α , and A are a constant, band gap, light frequency, Planck constant and absorption coefficient, respectively. The value of n is determined by the intrinsic optical transition properties of semiconductors, where $n = 4$ for indirect transition and $n = 1$ for direct transition [49]. In this work, the value of n equals 4 for indirect transition of CdS. As is shown in Fig. S4b, the band gap for pristine CdS is ~ 2.41 eV according to the equation, and comparatively ~ 2.37 eV for sample CC-20, which finally comes to the conclusion that cooperating CdS with CoO_x contributes to light absorption and possibly promotes the photocatalytic activities.

The efficiency of a heterogeneous photocatalytic system is also strongly correlated with the separation of photo induced electrons and

holes. Thereby steady-state photoluminescence spectra (PL) of CdS/CoO_x and pristine CdS are performed to investigate the effect of CoO_x on the surface structure and excited states of CdS NRs. As shown in Fig. 4b, either pristine CdS NRs or CdS/CoO_x core-shell NRs exhibit broad emission peaks around 520 nm with regard to the band to band transitions of the samples [50,51]. CdS/CoO_x core-shell NRs exhibit a similar PL spectrum with much weaker intensity compared to pristine CdS NRs, in which CC-20 exhibits the lowest intensity, indicating the excellent charge separation efficiency and the probable optimum photoactivity. The quenched PL intensity in CdS/CoO_x photocatalysts could be ascribed to the hole capturing effect of CoO_x, which further suppresses the recombination of electron-hole pairs and finally contribute to the photocatalytic activities [17,18,22].

To further investigate the effect of CoO_x on the enhanced charge separation efficiency, photoelectron current (PEC) experiments, as a simple and efficient technique to deeply investigate the optical properties, is conducted on a typical three-electrode cell in Na_2SO_4 aqueous solution under visible-light irradiation. Photocurrent is produced due to the diffusion of photogenerated electrons to the back contact and the capture of photogenerated holes by electron-donor in the electrolyte [52], which can be correlated with the generation and transfer of the photo excited charge carriers in the photocatalytic process [39]. As is concluded from Fig. 4c, there is a prominent improvement in photocurrent response of CdS/CoO_x core-shell NRs, suggesting that CoO_x promotes the separation of electron-hole pairs. Notably, CC-20 shows the strongest photocurrent response among the samples, also signifying the greatest charge separation efficiency in sample CC-20. Moreover, CdS/CoO_x NRs reveals relatively shorter diameters of semicircles of Nyquist plots (Fig. 4d), and expectedly CC-20 owns the shortest. This demonstrates the comparatively smaller charge transportation resistances in CdS/CoO_x NRs [53]. To sum up, speculations into PL and PEC results demonstrate the excellent charge separation efficiency of CdS/CoO_x NRs, in which the CoO_x layer acts as a crucial role of hole capturing and thus promoting the separation process.

In order to evaluate the efficacy of the CdS/CoO_x photocatalyst for

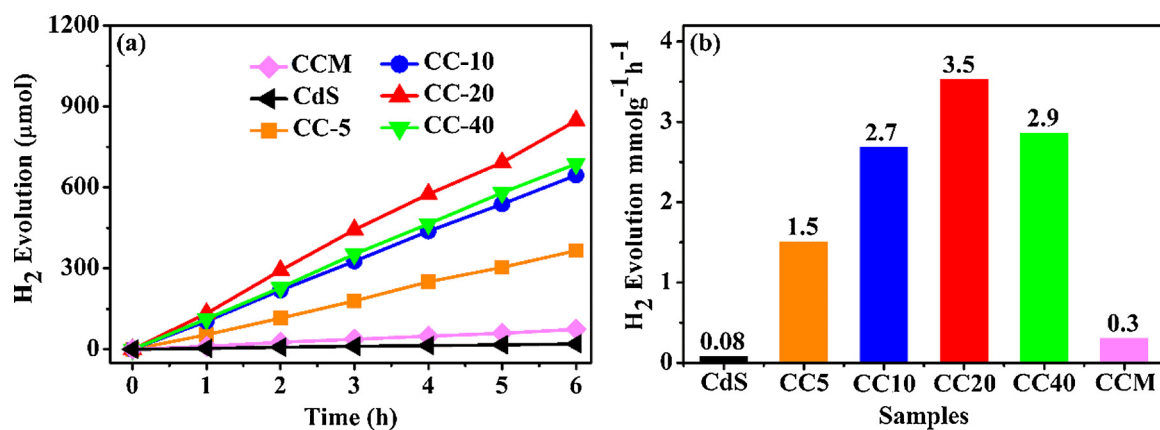


Fig. 5. a) Time courses of H₂ evolution of the samples and b) H₂ evolution rate of each sample.

hydrogen evolution, we intentionally implemented the hydrogen evolution experiment under aqueous condition using Na₂S and Na₂SO₃ as sacrificial agents. As is shown in Fig. 5a, merely no hydrogen is detected on any of the samples when there is no light ($\lambda > 420$ nm) irradiation, indicating that hydrogen evolution in this experiment is a photon-driven process. Additionally, the amount of hydrogen increases as the irradiation time extends, and CC-20 produces approximately 847.6 μmol of hydrogen in six hours, while only a trace amount of hydrogen (19.8 μmol) is produced on pristine CdS NRs.

We can conclude from Fig. 5b that pristine CdS shows a relative low H₂ production rate of about 0.08 mmol g⁻¹ h⁻¹, but notably CC-20 exhibit an optimal value up to 3.5 mmol g⁻¹ h⁻¹, which is about ca. 43-folds higher than that of pristine CdS NRs. Obviously, the optimal photocatalytic H₂ evolution activity of CC-20 among the as-prepared samples is in accordance with the PL and PEC results, demonstrating the crucial role of CoO_x in contributing to charge separation and thereby improves the photoactivities. Interestingly, further increasing the weight ratio of CoO_x deteriorates the overall efficiency of photocatalytic hydrogen evolution, which is probably due to the fact that excess amount of CoO_x coated on the surface of CdS NRs inhibits the light absorption of CdS, thus the photogenerated electron-hole pairs are severely diminished; moreover, the excess amount of CoO_x would also block the active sites on the surface of CdS NRs, yet hindering the reduction of H⁺ into hydrogen [54,55]. The properties of CC-40 provides complementary demonstrations for that, detailedly, CC-40 exhibit the highest light absorption ability among the samples in the wavelength over 500 nm but rather slower hydrogen evolution rate than CC-20, also indicating that light utilization is not the only driving force of the enhanced photoactivity.

Nevertheless, the core-shell structured CdS/CoO_x possesses much higher activity than the randomly deposited CdS/CoO_x, as can be concluded from the uncomparative photoactivity over CC-20 and CCM. This result reveals that the core-shell structure may also contributes to charge transportation and thus promotes the photocatalytic activities. To sum up, the improved charge separation and light absorption, along with the unique core-shell structure, may result in the greatly enhanced photoactivities.

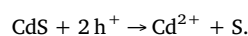
Cycling experiments are implemented to verify the stability of the catalyst. The photocatalytic hydrogen evolution cycling tests are carried out every six hours as one cycle, as depicted in Fig. S6. After 4 cycles, it can be clearly seen that there is a decline in photocatalytic hydrogen evolution activities of both pristine CdS and CC-20, which is possibly due to the severe photocorrosion of CdS according to the previously reported literatures [56,57]. However, there is a major difference behind the plummet. The photoactivity of CC-20 is reduced by nearly ca. 38% (Fig. S6a), but ca. 55% for pristine CdS NRs (Fig. S6b). This result demonstrates that CoO_x indeed inhibits the photocorrosion to a certain extent. Nevertheless, according to the XRD and FESEM data

of sample CC-20 irradiated after four cycles, neither any chemical composition nor structural collapse are observed. All the complementary characterizations evidently reveal the catalysts exhibited in this work a promising photocatalyst for water splitting.

Considering the prominent photocatalytic H₂ evolution capability and enhanced photostability achieved on CdS/CoO_x core-shell photocatalysts, it is indispensable to figure out the mechanism behind that. Generally, the overall efficiency of heterogenous systems are closely related with light absorption abilities, charge separation efficiency and their band gap potentials, etc. [58]. Based on the DRS results, we establish that the enhanced activity of the CdS/CoO_x core-shell nanorods correlates with a favorable light utilization compared to pristine CdS NRs. Broadened light absorption range manifests that more incident photons would be involved in the photocatalytic reactions, thus partially contribute to the photocatalytic activities. But the fact that CC-40 owns the strongest absorption ability at the wavelength longer than ~525 nm contradicts with the final photocatalytic H₂ evolution tests, in which CC-20 shows the optimum photoactivity. These results demonstrate that light absorption is not the only driving force of the enhanced photocatalytic activities, alternatively, charge separation may also play a crucial role in this.

As is show in Fig. 6, standpoints of the boosted charge separation provide more convincing explanations for the enhanced photocatalytic activities. In the first, due to the superior hole capture capability of CoO_x, charges are more efficiently separated during photocatalytic reactions, and redundant electrons left in CdS brings about higher photocatalytic hydrogen activities. And as clearly shown in the TEM results, a typical core-shell structure with large contacts between the CdS core and CoO_x shell is formed, which favor intimate junctions between the two species and drastically boosts the charge separation [59,60]. In this regard, rectified and reinforced charge transportation pathways of the core-shell structure predetermine the direction of charge flows, in other word, electrons and holes were directionally separated to the CdS core and CoO_x shell, thereby further inhibits the recombination of charge carriers. On the contrary, randomly deposited CoO_x result in a random flow of charges and a corresponding high recombination rate [25], as the outcomes revealed in the photocatalytic hydrogen evolution tests that CC-20 shows much higher photoactivities than CCM. Moreover, the large and intimately contacted CoO_x and CdS NRs elucidated from the XPS and TEM results give rise to more possible charge transportation pathways during photocatalytic process, which makes for more efficient hole transfer to some extent.

Nevertheless, it has been reported that the severe photocorrosion on CdS is closely related to the oxidation of photogenerated holes, which can be alternatively displayed in the following equation [16]:



And based on the above analysis, we assume that the enhanced

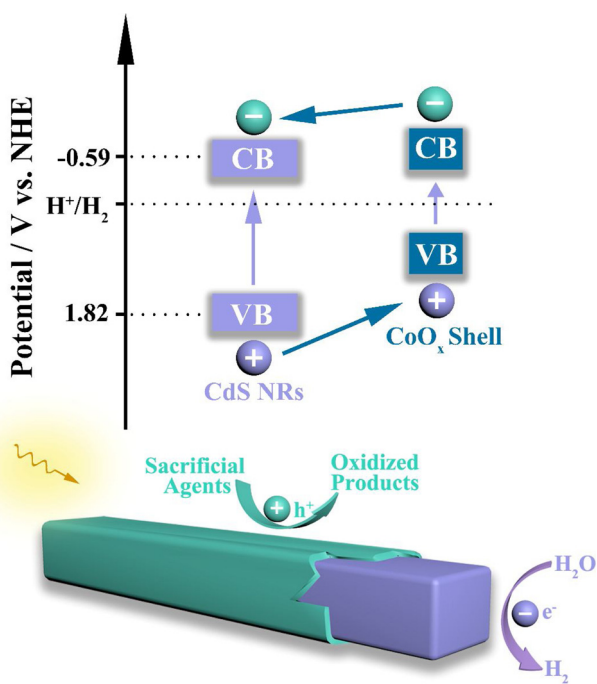


Fig. 6. Schematic diagram of the photocatalytic process over CdS/CoO_x NRs.

photostability is attributed to the prominent hole capturing effect of CoO_x as a typical oxidation co-catalyst. Precisely, the photogenerated holes are more preferable transported to the CoO_x outer shell and then consumed by sacrificial agents in the aqueous solution, therefore the photocorrosion is effectively inhibited.

According to the transformed Kubelka-Munk function and Valance Band XPS, the valance band and conduction band edges of CdS prepared in this work lies at 1.82 eV and -0.59 eV vs. NHE, while 0.49 eV and 1.11 eV for CoO_x. Ideally, the enhanced activity and stability could also be theoretically explained from the point of view of band alignment, as the energy band structure diagram illustrated in Fig. 5. When light is available, photogenerated electrons of CdS would be excited to the conduction band and correspondingly leave holes in valance band. Then, holes would be transferred to the CoO_x layer because of its hole capturing effect, and more electrons would be occupied in the conduction band of CdS, providing more reductive electrons employed for hydrogen evolution.

5. Conclusions

In summary, we intentionally design the novel core-shell structured CdS/CoO_x NRs via a facile impregnation-calcination method. The negatively charged surface directed the in situ growth of CoO and Co₃O₄, which finally transformed into an thin shell coated extrinsically on CdS NRs. Under the simultaneous action of the hole capturing effect of CoO_x and the unique core-shell structure, photogenerated holes are directionally transferred to the CoO_x shell, thus leading to a much higher charge separation efficiency. As a consequence, the sample obtained under optimum synthetic conditions exhibits several magnitudes higher hydrogen production rate and enhanced photostability compared to the pristine CdS NR. We believe that this work offers enlightenments on both the rectification of charge flows and stabilization of photocatalyst, and in the meanwhile makes for new paradigms for designing efficient solar energy conversion systems.

Acknowledgement

This work was supported by National Natural Science Foundation of China (201673300) and Hubei Provincial Natural Science Foundation

of China (2018CJB237).

Appendix A. Supplementary data

Supplementary material related to this article can be found, in the online version, at doi:<https://doi.org/10.1016/j.apcatb.2018.04.037>.

References

- X.C. Wang, K. Maeda, A. Thomas, K. Takanabe, G. Xin, J.M. Carlsson, K. Domen, M. Antonietti, *Nat. Mater.* 8 (2009) 76–80.
- W. Hu, L. Lin, R.Q. Zhang, C. Yang, J.L. Yang, *J. Am. Chem. Soc.* 139 (2017) 15429–15436.
- Y.J. Cao, S. Chen, Q.Q. Luo, H. Yan, Y. Lin, W. Liu, L.L. Cao, J.L. Lu, J.L. Yang, T. Yao, S.Q. Wei, *Angew. Chem. Int. Ed.* 56 (2017) 12191–12196.
- J. Liu, Y. Liu, N.Y. Liu, Y.Z. Han, X. Zhang, H. Huang, Y. Lifshitz, S.T. Lee, J. Zhong, Z.H. Kang, *Science* 347 (2015) 970–974.
- S.S. Chen, T. Takata, K. Domen, *Nat. Rev. Mater.* 2 (2017) 17050.
- Z.Z. Cheng, F.M. Wang, T.A. Shifa, C. Jiang, Q.L. Liu, J. He, *Small* 13 (2017) 1702163.
- F.F. Wang, Q. Li, D.S. Xu, *Adv. Energy Mater.* (2017) 1700529.
- J. Qi, W. Zhang, R. Cao, *Adv. Energy Mater.* 8 (2017) 1701620.
- K. Takanabe, *ACS Catal.* 7 (2017) 8006–8022.
- B.C. Qiu, Q.H. Zhu, M.M. Du, L.G. Fan, M.Y. Xing, J.L. Zhang, *Angew. Chem. Int. Ed.* 56 (2017) 2684–2688.
- T. Simon, N. Bouchonville, M.J. Berr, A. Vaneski, A. Adrovic, D. Volbers, R. Wyrwicz, M. Doblinger, A.S. Susha, A.L. Rogach, F. Jackel, J.K. Stolarczyk, J. Feldmann, *Nat. Mater.* 13 (2014) 1–6.
- N.Z. Bao, L.M. Shen, T. Takata, K. Domen, *Chem. Mater.* 20 (2008) 110–117.
- M. Luo, Y. Liu, J.C. Hu, H. Liu, J.L. Li, *ACS Appl. Mater. Interfaces* 4 (2012) 1813–1821.
- F. Yang, N.N. Yan, S. Huang, Q. Sun, L.Z. Zhang, Y. Yu, *J. Phys. Chem. C* 116 (2012) 9078–9084.
- J.R. Ran, J. Zhang, J.G. Yu, M. Jaroniec, S.Z. Qiao, *Chem. Soc. Rev.* 43 (2014) 7787–7812.
- J.H. Yang, D. Wang, H.X. Han, C. Li, *Acc. Chem. Res.* 46 (2013) 1900–1909.
- A. Yamakata, M. Kawaguchi, N. Nishimura, T. Minegishi, J. Kubota, K. Domen, *J. Phys. Chem. C* 118 (2014) 23897–23906.
- S. Li, L.B. Hou, L.J. Zhang, L.P. Chen, Y.H. Lin, D.J. Wang, T.F. Xie, *J. Mater. Chem. A* 3 (2015) 17820–17826.
- E. Nurlaela, S. Ould-Chikh, I. Llorens, J.L. Hazemann, K. Takanabe, *Chem. Mater.* 27 (2015) 5685–5694.
- S.M. Fang, S.S. Li, L. Ge, C.C. Han, P. Qiu, Y.Q. Gao, *Dalton Trans.* 46 (2017) 10578–10585.
- D.A. Wang, T. Hisatomi, T. Takata, C.S. Pan, M. Katayama, J. Kubota, K. Domen, *Angew. Chem. Int. Ed.* 52 (2013) 11252–11256.
- J.K. Zhang, Z.B. Yu, Z. Gao, H.B. Ge, S.C. Zhao, C.Q. Chen, S.A. Chen, X.L. Tong, M.H. Wang, Z.F. Zheng, Y. Qin, *Angew. Chem. Int. Ed.* 56 (2017) 816–820.
- Y.G. Chen, S. Zhao, X. Wang, Q. Peng, R. Lin, Y. Wang, R.A. Shen, X. Gao, L.B. Zhang, G. Zhou, J. Li, A.D. Xia, Y.D. Li, *J. Am. Chem. Soc.* 138 (2016) 4286–4289.
- M.Y. Xing, B.C. Qiu, M.M. Du, Q.H. Zhu, L.Z. Wang, J.L. Zhang, *Adv. Funct. Mater.* 27 (2017) 1702624.
- Z. Wang, W.W. Wu, Q. Xu, G.D. Li, S.H. Liu, X.F. Jia, Y. Qin, Z.L. Wang, *Nano Energy* 38 (2017) 518–525.
- S.S. Chen, S. Shen, G.J. Liu, Y. Qi, F.X. Zhang, C. Li, *Angew. Chem. Int. Ed.* 54 (2015) 3047–3051.
- J. Liu, J. Meeprasert, S. Namuangruk, K.W. Zha, H.R. Li, L. Huang, P. Maitarad, L.Y. Shi, D.S. Zhang, *J. Phys. Chem. C* 121 (2017) 4970–4979.
- J. Han, J. Meeprasert, P. Maitarad, S. Namuangruk, L.Y. Shi, D.S. Zhang, *J. Phys. Chem. C* 120 (2016) 1523–1533.
- Q. Li, H. Meng, P. Zhou, Y.Q. Zheng, J. Wang, J.G. Yu, J.R. Gong, *ACS Catal.* 3 (2013) 882–889.
- X.Y. Zhang, Z. Zhao, W.W. Zhang, G.Q. Zhang, D. Qu, X. Miao, S.R. Sun, Z.C. Sun, *Small* 12 (2016) 793–801.
- Q.Z. Wang, J.J. Li, Y. Bai, J.H. Lian, H.H. Huang, Z.M. Li, Z.Q. Lei, W.F. Shuangguan, *Green Chem.* 16 (2014) 2728–2735.
- R.D. Seals, R. Alexander, L.T. Taylor, J.G. Dillard, *Inorg. Chem.* 12 (1973) 2485–2487.
- K. Zhang, J.K. Kim, B. Park, S.F. Qian, B.J. Jin, X.W. Sheng, H.B. Zeng, H.J. Shin, S.H. Oh, C.L. Lee, J.H. Park, *Nano Lett.* 17 (2017) 6676–6683.
- X.F. Liu, X.Y. Xiong, S.P. Ding, Q.Q. Jiang, J.C. Hu, *Catal. Sci. Technol.* 7 (2017) 3580–3590.
- Y.Q. Shi, X.Y. Xiong, S.P. Ding, X.F. Liu, Q.Q. Jiang, J.C. Hu, *Appl. Catal. B: Environ.* 220 (2018) 570–580.
- M.C. Biesinger, B.P. Payne, A.P. Grosvenor, L.W.M. Lau, A.R. Gerson, R.S.C. Smart, *Appl. Surf. Sci.* 257 (2011) 2717–2730.
- M.M. Han, H.B. Wang, S.Q. Zhao, L.L. Hu, H. Huang, Y. Liu, *Inorg. Chem. Front.* 4 (2017) 1691–1696.
- M. Khasu, T. Nyathi, D.J. Morgan, G.J. Hutchings, M. Claeys, N. Fischer, *Catal. Sci. Technol.* 7 (2017) 4806–4817.
- S.P. Ding, X.Y. Xiong, X.F. Liu, Y.Q. Shi, Q.Q. Jiang, J.C. Hu, *Catal. Sci. Technol.* 7 (2017) 3791–3801.

[40] J.W. Huang, Y. Zhang, Y. Ding, *ACS Catal.* 7 (2017) 1841–1845.

[41] L. Huang, X.N. Hu, S. Yuan, H.R. Li, T.T. Yan, L.Y. Shi, D.S. Zhang, *Appl. Catal. B: Environ.* 203 (2017) 778–788.

[42] L. Liao, Q.H. Zhang, Z.H. Su, Z.Z. Zhao, Y.N. Wang, Y. Li, X.X. Lu, D.G. Wei, G.Y. Feng, Q.K. Yu, X.J. Cai, J.M. Zhao, Z.F. Ren, H. Fang, F. Robles-Hernandez, S. Baldelli, J.M. Bao, *Nat. Nanotechnol.* 9 (2014) 69–73.

[43] J.Q. Guan, C.M. Ding, R.T. Chen, B.K. Huang, X.W. Zhang, F.T. Fan, F.X. Zhang, C. Li, *Chem. Sci.* 8 (2017) 6111–6116.

[44] L.J. Zhang, S. Li, B.K. Liu, D.J. Wang, T.F. Xie, *ACS Catal.* 4 (2014) 3724–3729.

[45] D. Barreca, C. Massignan, S. Daolio, M. Fabrizio, C. Piccirillo, L. Armelao, E. Tondello, *Chem. Mater.* 13 (2001) 588–593.

[46] G. George, S. Anandhan, *RSC Adv.* 5 (2015) 81429–71437.

[47] R.G. Li, Z. Chen, W. Zhao, F.X. Zhang, K. Maeda, B.K. Huang, S. Shen, K. Domen, C. Li, *J. Phys. Chem. C* 117 (2012) 376–382.

[48] C.W. Yang, J.Q. Qin, Z. Xue, M.Z. Ma, X.Y. Zhang, R.P. Liu, *Nano Energy* 41 (2017) 1–9.

[49] X.C. Meng, Z.Z. Li, H.M. Zeng, J. Chen, Z.S. Zhang, *Appl. Catal. B: Environ.* 210 (2017) 160–172.

[50] R. Shi, H.F. Ye, F.L. iang, Z. Wang, K. Li, Y.X. Weng, Z.S. Lin, W.F. Fu, C.M. Che, Y. Chen, *Adv. Mater.* 30 (2018) 1705941.

[51] X.L. Xu, Y.Y. Zhao, E.J. Sie, Y.H. Lu, B. Liu, S.A. Ekahana, X. Ju, Q.K. Jiang, J.B. Wang, H.D. Sun, T.C. Sum, C.H.A. Huan, Y.P. Feng, Q.H. Xiong, *ASC Nano* 5 (2011) 3660–3669.

[52] F.X. Xiao, S.F. Hung, J.W. Miao, H.Y. Wang, H.B. Yang, B. Liu, *Small* 11 (2015) 554–567.

[53] B. Tian, W.L. Zhen, H.B. Gao, X.Q. Zhang, Z. Li, G.X. Lu, *Appl. Catal. B: Environ.* 203 (2017) 789–797.

[54] A. Dickinson, D. James, N. Perkins, T. Cassidy, M. Bowker, *J. Mol. Catal. A: Chem.* 146 (1999) 211–221.

[55] J. Zhang, S.Z. Qiao, L.F. Qi, J.G. Yu, *Phys. Chem. Chem. Phys.* 15 (2013) 12088–12094.

[56] D. Meissner, R. Memming, B. Kastening, *J. Phys. Chem.* 92 (1988) 3476–3483.

[57] D. Meissner, C. Bennedorf, R. Memming, *Appl. Surf. Sci.* 27 (1987) 423–436.

[58] N.S. Lewis, *Nanotechnol.* 11 (2016) 1010–1019.

[59] B. Han, S.Q. Liu, N. Zhang, Y.J. Xu, Z.R. Tang, *Appl. Catal. B: Environ.* 202 (2017) 298–304.

[60] Z.Z. Wu, Y.F. Jiang, X.Y. Xiong, S.P. Ding, Y.Q. Shi, X.F. Liu, Y. Liu, Z.X. Huang, J.C. Hu, *Catal. Sci. Technol.* 7 (2017) 3464–3468.